

Search for lepton-flavor-violating $\tau \rightarrow \ell V^0$ decays at Belle

Y. Nishio,²⁰ K. Inami,²⁰ T. Ohshima,²⁰ I. Adachi,⁷ H. Aihara,⁴¹ K. Arinstein,¹ V. Aulchenko,¹ T. Aushev,^{16, 11}
T. Aziz,³⁷ A. M. Bakich,³⁶ V. Balagura,¹¹ E. Barberio,¹⁹ I. Bedny,¹ K. Belous,⁹ U. Bitenc,¹² S. Blyth,²³
A. Bondar,¹ M. Bračko,^{7, 18, 12} T. E. Browder,⁶ A. Chen,²² W. T. Chen,²² B. G. Cheon,⁵ I.-S. Cho,⁴⁵ Y. Choi,³⁵
J. Dalseno,¹⁹ M. Danilov,¹¹ M. Dash,⁴⁴ A. Drutskoy,³ S. Eidelman,¹ D. Epifanov,¹ N. Gabyshev,¹ B. Golob,^{17, 12}
H. Ha,¹⁴ J. Haba,⁷ K. Hara,²⁰ K. Hayasaka,²⁰ H. Hayashii,²¹ M. Hazumi,⁷ Y. Horii,⁴⁰ Y. Hoshi,³⁹
W.-S. Hou,²⁴ Y. B. Hsiung,²⁴ T. Iijima,²⁰ A. Ishikawa,³² R. Itoh,⁷ M. Iwasaki,⁴¹ Y. Iwasaki,⁷ N. J. Joshi,³⁷
D. H. Kah,¹⁵ H. Kaji,²⁰ J. H. Kang,⁴⁵ N. Katayama,⁷ H. Kawai,² T. Kawasaki,²⁷ H. Kichimi,⁷ Y. J. Kim,⁴
S. Korpar,^{18, 12} Y. Kozakai,²⁰ P. Križan,^{17, 12} P. Krokovny,⁷ R. Kumar,³¹ C. C. Kuo,²² Y. Kuroki,³⁰ A. Kuzmin,¹
Y.-J. Kwon,⁴⁵ J. S. Lee,³⁵ M. J. Lee,³⁴ S. E. Lee,³⁴ T. Lesiak,²⁵ A. Limosani,¹⁹ Y. Liu,⁴ D. Liventsev,¹¹
F. Mandl,¹⁰ S. McOnie,³⁶ H. Miyake,³⁰ H. Miyata,²⁷ Y. Miyazaki,²⁰ R. Mizuk,¹¹ G. R. Moloney,¹⁹ T. Mori,²⁰
E. Nakano,²⁹ M. Nakao,⁷ H. Nakazawa,²² S. Nishida,⁷ O. Nitoh,⁴³ S. Ogawa,³⁸ S. Okuno,¹³ H. Ozaki,⁷ P. Pakhlov,¹¹
G. Pakhlova,¹¹ C. W. Park,³⁵ H. Park,¹⁵ R. Pestotnik,¹² L. E. Piilonen,⁴⁴ A. Poluektov,¹ Y. Sakai,⁷
O. Schneider,¹⁶ K. Senyo,²⁰ M. E. Sevir,¹⁹ M. Shapkin,⁹ V. Shebalin,¹ H. Shibuya,³⁸ J.-G. Shiu,²⁴ B. Shwartz,¹
J. B. Singh,³¹ A. Sokolov,⁹ A. Somov,³ S. Stanič,²⁸ M. Starič,¹² T. Sumiyoshi,⁴² F. Takasaki,⁷ M. Tanaka,⁷
G. N. Taylor,¹⁹ Y. Teramoto,²⁹ I. Tikhomirov,¹¹ S. Uehara,⁷ K. Ueno,²⁴ T. Uglov,¹¹ Y. Unno,⁵ S. Uno,⁷
Y. Usov,¹ G. Varner,⁶ S. Villa,¹⁶ A. Vinokurova,¹ C. H. Wang,²³ P. Wang,⁸ X. L. Wang,⁸ Y. Watanabe,¹³
E. Won,¹⁴ Y. Yamashita,²⁶ Z. P. Zhang,³³ V. Zhilich,¹ V. Zhulanov,¹ A. Zupanc,¹² and O. Zyukova¹

(The Belle Collaboration)

¹*Budker Institute of Nuclear Physics, Novosibirsk, Russia*

²*Chiba University, Chiba, Japan*

³*University of Cincinnati, Cincinnati, OH, USA*

⁴*The Graduate University for Advanced Studies, Hayama, Japan*

⁵*Hanyang University, Seoul, South Korea*

⁶*University of Hawaii, Honolulu, HI, USA*

⁷*High Energy Accelerator Research Organization (KEK), Tsukuba, Japan*

⁸*Institute of High Energy Physics, Chinese Academy of Sciences, Beijing, PR China*

⁹*Institute for High Energy Physics, Protvino, Russia*

¹⁰*Institute of High Energy Physics, Vienna, Austria*

¹¹*Institute for Theoretical and Experimental Physics, Moscow, Russia*

¹²*J. Stefan Institute, Ljubljana, Slovenia*

¹³*Kanagawa University, Yokohama, Japan*

¹⁴*Korea University, Seoul, South Korea*

¹⁵*Kyungpook National University, Taegu, South Korea*

¹⁶*École Polytechnique Fédérale de Lausanne, EPFL, Lausanne, Switzerland*

¹⁷*Faculty of Mathematics and Physics, University of Ljubljana, Ljubljana, Slovenia*

¹⁸*University of Maribor, Maribor, Slovenia*

¹⁹*University of Melbourne, Victoria, Australia*

²⁰*Nagoya University, Nagoya, Japan*

²¹*Nara Women's University, Nara, Japan*

²²*National Central University, Chung-li, Taiwan*

²³*National United University, Miao Li, Taiwan*

²⁴*Department of Physics, National Taiwan University, Taipei, Taiwan*

²⁵*H. Niewodniczanski Institute of Nuclear Physics, Krakow, Poland*

²⁶*Nippon Dental University, Niigata, Japan*

²⁷*Niigata University, Niigata, Japan*

²⁸*University of Nova Gorica, Nova Gorica, Slovenia*

²⁹*Osaka City University, Osaka, Japan*

³⁰*Osaka University, Osaka, Japan*

³¹*Panjab University, Chandigarh, India*

³²*Saga University, Saga, Japan*

³³*University of Science and Technology of China, Hefei, PR China*

³⁴*Seoul National University, Seoul, South Korea*

³⁵*Sungkyunkwan University, Suwon, South Korea*

³⁶*University of Sydney, Sydney, NSW, Australia*

³⁷Tata Institute of Fundamental Research, Mumbai, India

³⁸Toho University, Funabashi, Japan

³⁹Tohoku Gakuin University, Tagajo, Japan

⁴⁰Tohoku University, Sendai, Japan

⁴¹Department of Physics, University of Tokyo, Tokyo, Japan

⁴²Tokyo Metropolitan University, Tokyo, Japan

⁴³Tokyo University of Agriculture and Technology, Tokyo, Japan

⁴⁴Virginia Polytechnic Institute and State University, Blacksburg, VA, USA

⁴⁵Yonsei University, Seoul, South Korea

We have searched for neutrinoless τ lepton decays into ℓ and V^0 , where ℓ stands for an electron or muon, and V^0 for a vector meson (ϕ , ω , K^{*0} , \bar{K}^{*0} or ρ^0), using 543 fb^{-1} of data collected with the Belle detector at the KEKB asymmetric-energy e^+e^- collider. No excess of signal events over the expected background has been observed, and we set upper limits on the branching fractions in the range $(5.9 - 18) \times 10^{-8}$ at the 90% confidence level. These upper limits include the first results for the $\ell\omega$ mode as well as new limits that are significantly more restrictive than our previous results for the $\ell\phi$, ℓK^{*0} , $\ell\bar{K}^{*0}$ and $\ell\rho^0$ modes.

PACS numbers: 11.30.Fs, 13.35.Dx, 14.60.Fg

INTRODUCTION

In the Standard Model (SM), lepton-flavor-violating (LFV) decays of charged leptons are forbidden; even if neutrino mixing is taken into account, they are highly suppressed. However, LFV is expected to appear in many extensions of the SM. Some such models predict branching fractions for τ LFV decays in the range $10^{-8} - 10^{-7}$ [1, 2, 3], which can be reached at the present B-factories. An observation of LFV would provide unambiguous evidence for new physics beyond the SM.

A search for LFV τ^- decays into neutrinoless final states with one charged lepton ℓ^- (e^- or μ^-) and a vector meson was first performed by the CLEO collaboration in the $\ell^-\phi$, ℓ^-K^{*0} , $\ell^-\bar{K}^{*0}$ and $\ell^-\rho^0$ final states in 1998; this search set upper limits in the range $(2.0 - 7.5) \times 10^{-6}$ [4]. Later, Belle obtained upper limits in the range $(2.0 - 7.7) \times 10^{-7}$ using 158 fb^{-1} of data. In this paper, we report an improved search for LFV τ^- decays [5] into a charged lepton and a neutral vector meson (V^0), where V^0 includes ω in addition to the ϕ , K^{*0} , \bar{K}^{*0} and ρ^0 [†]. The analysis is based on a data sample of 543 fb^{-1} , corresponding to 4.99×10^8 τ -pairs collected with the Belle detector [7] at the KEKB asymmetric-energy e^+e^- collider [8] taken at the $\Upsilon(4S)$ resonance and 60 MeV below it. These results supersede our previous published results [9].

The Belle detector is a large-solid-angle magnetic spectrometer that consists of a silicon vertex detector, a 50-layer central drift chamber, an array of aerogel threshold Cherenkov counters, a barrel-like arrangement of time-of-flight scintillation counters, and an electromagnetic

calorimeter comprised of CsI(Tl) crystals located inside a superconducting solenoid coil that provides a 1.5 T magnetic field. An iron flux-return located outside the coil is instrumented to detect K_L^0 mesons and to identify muons. The detector is described in detail elsewhere [7]. Two inner detector configurations were used. A 2.0 cm radius beam-pipe and a 3-layer silicon vertex detector were used for the first sample of 158 fb^{-1} , while a 1.5 cm radius beam-pipe, a 4-layer silicon detector and a small-cell inner drift chamber were used to record the remaining 385 fb^{-1} [10].

EVENT SELECTION

We search for events, in which one τ decays to a charged lepton and two charged hadrons (3-prong decay) while the other τ decays into one charged particle (1-prong decay) and missing neutral particle(s). We reconstruct ϕ candidates from K^+K^- , ω from $\pi^+\pi^-\pi^0$, K^{*0} from $K^+\pi^-$, \bar{K}^{*0} from $K^-\pi^+$ and ρ^0 from $\pi^+\pi^-$.

The selection criteria described below are optimized from studies of Monte Carlo (MC) simulated events and the experimental data distributions. The background estimation is based on MC simulations of the reaction $e^+e^- \rightarrow \tau^+\tau^-$ as well as $q\bar{q}$ continuum and two-photon processes. The $\tau^+\tau^-$ sample corresponding to 1524 fb^{-1} is generated using the KKMC code [11]. The MC samples of $q\bar{q}$ and two-photon processes are produced using EvtGen [12] and AAFH [13], respectively, in amounts corresponding to the luminosity of the experiment. The signal MC events are generated by KKMC assuming a phase-space distribution for τ decay. The detector response is simulated by a GEANT3 [14] based program.

The transverse momentum for each charged track is required to be larger than $0.06 \text{ GeV}/c$ in the barrel region ($-0.6235 < \cos\theta < 0.8332$, where θ is the polar angle relative to the direction opposite to that of the incident

[†] While preparing this paper, we became aware that the BaBar group had also reported on a search for $\tau^- \rightarrow \ell^-\omega$ in a preprint [6].

e^+ beam in the laboratory frame) and 0.1 GeV/c in the endcap region ($-0.8660 < \cos\theta < -0.6235$ and $0.8332 < \cos\theta < 0.9563$). The energies of photon candidates are required to be larger than 0.1 GeV in both regions.

To select the signal topology, we require four charged tracks in an event with zero net charge, and the total energy of charged tracks and photons in the center-of-mass (CM) frame to be less than 11 GeV. We also require the missing momentum in the laboratory frame to exceed 0.6 GeV/c, and to point into the detector acceptance ($-0.8660 < \cos\theta < 0.9563$). Here the missing momentum is defined as the difference between the momentum of the initial e^+e^- system, and the sum of the observed momentum vectors. An event is subdivided into 3-prong and 1-prong hemispheres with respect to the thrust axis calculated from the momenta of all charged tracks and photons in the CM frame. These hemispheres are referred to as the signal and tag sides, respectively. We allow at most two photons on the tag side to take into account initial state radiation. To reduce the $q\bar{q}$ background, not more than one photon on the signal side is allowed for the $\ell^-\phi$, ℓ^-K^{*0} , $\ell^-\bar{K}^{*0}$, $\ell^-\rho^0$ modes while not more than two photons in addition to π^0 daughters are permitted for the $\ell^-\omega$ modes. A charged particle of the type x ($x = \mu, e, K$ or π) is identified using the likelihood ratio parameter, P_x . This is defined as $P_x = L_x / (\sum_x L_x)$, where L_x is the likelihood for particle type x , determined from the responses of the relevant detectors [15]. For muon candidates on the signal side we require $P_\mu > 0.95$ while their momentum should be greater than 1.0 GeV/c. The efficiency for muon identification is 92% with a 1.2% probability to misidentify a pion as a muon. Electrons on the signal side are required to have $P_e > 0.9$ and momenta greater than 0.5 GeV/c. The efficiency for the electron identification is 94% while the probability to misidentify a pion as an electron is 0.1%.

Candidate ϕ mesons are selected from K^+K^- pairs with invariant mass in the range $1.01 \text{ GeV}/c^2 < M_{K^+K^-} < 1.03 \text{ GeV}/c^2$ ($\pm 4\sigma$). For both kaon daughters we require $P_K > 0.8$. To reduce the background from the $\gamma \rightarrow e^+e^-$ conversions the cut $P_e < 0.1$ is applied.

Candidate ω mesons are reconstructed from $\pi^+\pi^-\pi^0$ with the invariant mass requirement $0.757 \text{ GeV}/c^2 < M_{\pi^+\pi^-\pi^0} < 0.808 \text{ GeV}/c^2$ ($\pm 3\sigma$). A π^0 candidate is selected from γ pairs with invariant mass in the range $0.11 \text{ GeV}/c^2 < M_{\gamma\gamma} < 0.15 \text{ GeV}/c^2$. In order to improve the ω mass resolution, the π^0 mass is constrained to its world average value of $134.9766 \text{ GeV}/c^2$ for the ω mass reconstruction.

Candidate K^{*0} and \bar{K}^{*0} mesons are selected from $K^\pm\pi^\mp$ pairs with invariant mass in the range $0.827 \text{ GeV}/c^2 < M_{K\pi} < 0.968 \text{ GeV}/c^2$ ($\pm 3\sigma$), which satisfy the condition $P_K > 0.8$ for the kaon candidate and $P_e < 0.1$ for both daughters.

Candidate ρ^0 mesons are selected from $\pi^+\pi^-$ pairs with invariant mass in the range $0.478 \text{ GeV}/c^2 <$

$M_{\pi^+\pi^-} < 1.074 \text{ GeV}/c^2$ ($\pm 4\sigma$), requiring that the daughter pions have $P_K < 0.1$, $P_e < 0.1$ and momenta greater than 0.5 GeV/c. In addition, for the $\tau^- \rightarrow e^-\rho^0$ mode, we require $P_\mu < 0.5$ for daughter pions in order to reduce the two-photon background from $ee \rightarrow ee\mu\mu$.

Figures 1 (a)-(d) show the invariant mass distributions of the ϕ , ω , K^{*0} and ρ^0 candidates for the $\tau^- \rightarrow \mu^-\phi$, $\tau^- \rightarrow \mu^-\omega$, $\tau^- \rightarrow \mu^-K^{*0}$ and $\tau^- \rightarrow \mu^-\rho^0$ modes, respectively. The estimated background distributions agree with the data. The main background contribution for the $\tau^- \rightarrow \ell^-\phi$ mode is due to $q\bar{q}$ events involving ϕ mesons. For the $\tau^- \rightarrow \ell^-\omega$ mode the dominant background comes from $\tau^- \rightarrow \pi^-\omega\nu_\tau$ decay with the pion misidentified as a lepton. The $\tau^- \rightarrow \pi^-\pi^+\pi^-\nu_\tau$ decay is one of the main background sources for the $\tau^- \rightarrow \ell^-K^{*0}$, $\ell^-\bar{K}^{*0}$ and $\tau^- \rightarrow \ell^-\rho^0$ modes. In this background source one pion is misidentified as a lepton for all modes while for the $\tau^- \rightarrow \ell^-K^{*0}$ and $\ell^-\bar{K}^{*0}$ modes one additional pion is misidentified as a kaon.

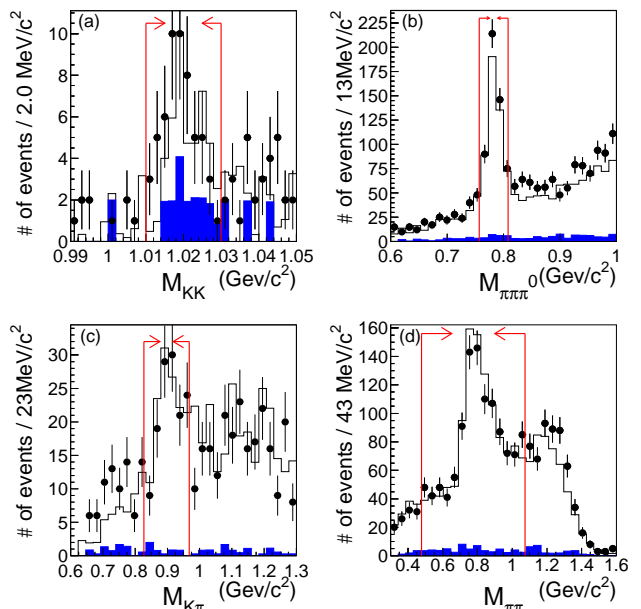


FIG. 1: Invariant mass distributions of (a) $\phi \rightarrow K^+K^-$ for $\tau^- \rightarrow \mu^-\phi$, (b) $\omega \rightarrow \pi^+\pi^-\pi^0$ for $\tau^- \rightarrow \mu^-\omega$, (c) $K^{*0} \rightarrow K^+\pi^-$ for $\tau^- \rightarrow \mu^-K^{*0}$ and (d) $\rho^0 \rightarrow \pi^+\pi^-$ for $\tau^- \rightarrow \mu^-\rho^0$ in the region $1.5 \text{ GeV}/c^2 < M_{\ell\nu^0} < 1.95 \text{ GeV}/c^2$ and $-0.5 \text{ GeV} < \Delta E < 0.5 \text{ GeV}$. The points with error bars are data. The open histogram shows the expected $\tau^+\tau^-$ background MC while the filled histogram is the sum of $q\bar{q}$ and two-photon MCs. The regions between the vertical lines are selected.

To reduce the remaining background from $\tau^+\tau^-$ and $q\bar{q}$, the events from the triangular area defined by the missing momentum, p_{miss} (GeV/c), and missing mass squared, m_{miss}^2 ((GeV/c²)²) are selected for further consideration. These requirements are summarized in Table I and illustrated in Fig. 2 by the two-dimensional plots of p_{miss} (GeV/c) versus m_{miss}^2 ((GeV/c²)²) for the

TABLE I: Selection criteria using p_{miss} (GeV/c) and m_{miss}^2 ($(\text{GeV}/c^2)^2$) where p_{miss} is missing momentum and m_{miss}^2 is missing mass squared.

Mode	Selection criteria
$\tau^- \rightarrow$	
$\ell^- \phi$	$p_{\text{miss}} > \frac{8}{9} m_{\text{miss}}^2$ and $m_{\text{miss}}^2 > -0.5$
$\ell^- \omega$	$p_{\text{miss}} > \frac{8}{3} m_{\text{miss}}^2 - \frac{1}{3} \frac{p_{\text{miss}}}{\cos \theta_{\ell\omega}^{\text{CM}}}$ and $m_{\text{miss}}^2 > -0.5$
$\mu^- K^{*0}$	$p_{\text{miss}} > \frac{8}{4.5} m_{\text{miss}}^2 - \frac{1}{11} \frac{p_{\text{miss}}}{\cos \theta_{\ell K^{*0}}^{\text{CM}}}$ and $p_{\text{miss}} > 8m_{\text{miss}}^2$
$e^- K^{*0}$	$p_{\text{miss}} > \frac{8}{5.5} m_{\text{miss}}^2 - \frac{1}{11} \frac{p_{\text{miss}}}{\cos \theta_{\ell K^{*0}}^{\text{CM}}}$ and $m_{\text{miss}}^2 > 0$
$\mu^- \bar{K}^{*0}$	$p_{\text{miss}} > \frac{8}{6.5} m_{\text{miss}}^2$ and $m_{\text{miss}}^2 > -0.5$
$e^- \bar{K}^{*0}$	$p_{\text{miss}} > \frac{8}{5} m_{\text{miss}}^2$ and $p_{\text{miss}} > -\frac{8}{1.4} m_{\text{miss}}^2$
$\mu^- \rho^0$	$p_{\text{miss}} > -8m_{\text{miss}}^2 - 4$ and $p_{\text{miss}} > 2m_{\text{miss}}^2$
$e^- \rho^0$	$p_{\text{miss}} > -8m_{\text{miss}}^2 - 4$ and $p_{\text{miss}} > 1.6m_{\text{miss}}^2$

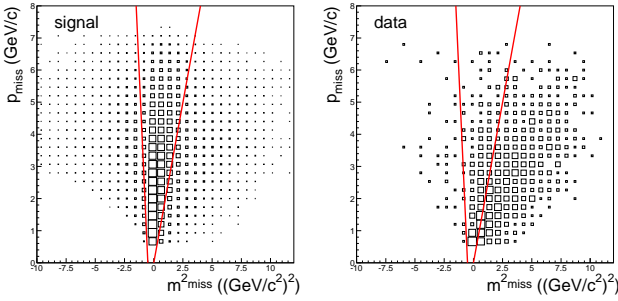


FIG. 2: p_{miss} vs. m_{miss}^2 plots for signal MC and data for the $\tau \rightarrow \mu \rho^0$ mode. The regions between the vertical lines are selected.

$\tau^- \rightarrow \mu^- \rho^0$ mode.

For the $\ell^- \omega$ ($\ell^- K^{*0}$ and $\ell^- \bar{K}^{*0}$) mode, we require that the opening angle between the lepton and ω (K^{*0}) on the signal side in the CM frame, $\theta_{\ell\omega}^{\text{CM}}$ ($\theta_{\ell K^{*0}}^{\text{CM}}$), satisfy $\cos \theta_{\ell\omega}^{\text{CM}} < 0.88$ ($\cos \theta_{\ell K^{*0}}^{\text{CM}} < 0.93$). To remove two-photon background for the eV^0 modes, we further require that the opening angle, α , between the direction of the total momentum of charged tracks and γ 's on the signal side and that on the tag side satisfy the condition $\cos \alpha > -0.999$ for the $e^- \phi$, $\cos \alpha > -0.996$ for the $e^- \omega$, $e^- K^{*0}$ (\bar{K}^{*0}) and $\cos \alpha > -0.990$ for the $e^- \rho^0$ mode.

To identify signal τ decays, we reconstruct the ℓV^0 invariant mass, $M_{\ell V^0}$, and the energy difference in the CM frame, ΔE , between the sum of energies on the signal side and the beam-energy, E_{beam} . Signal events should concentrate around $M_{\ell V^0} = m_\tau$ and $\Delta E = 0$, where m_τ is the nominal τ mass. For the $\ell\omega$ modes, we used the beam-energy constrained mass, M_{bc} , instead of the invariant mass M_{inv} , where $M_{\text{bc}} = \sqrt{E_{\text{beam}}^2 - (\vec{p}_\tau)^2}$, in order to improve the mass resolution, which is smeared due to the γ energy resolution. In calculating the τ momentum \vec{p}_τ , we replace the magnitude of the π^0 momentum with the value obtained from the beam energy, the energies of charged tracks on the signal side and the π^0

direction measured by the calorimeter.

The resolutions in ΔE and $M_{\ell V^0}$, evaluated using the signal MC, are summarized in Table II. We define the signal region in the $\Delta E - M_{\ell V^0}$ plane as a $\pm 3\sigma$ ellipse. In order to avoid biases in the event selection, we blind the signal region until the analysis is finalized.

TABLE II: Resolutions in $M_{\ell V^0}$ in MeV/c^2 and ΔE in MeV . The superscripts low and high indicate the lower and higher sides of the peak, respectively.

Mode	$\sigma_{M_{\ell V^0}}^{\text{high}}$	$\sigma_{M_{\ell V^0}}^{\text{low}}$	$\sigma_{\Delta E}^{\text{high}}$	$\sigma_{\Delta E}^{\text{low}}$
$\tau^- \rightarrow$				
$\mu^- \phi$	3.4 ± 0.2	3.4 ± 0.2	13.2 ± 0.4	14.0 ± 0.5
$e^- \phi$	3.7 ± 0.1	3.6 ± 0.1	13.3 ± 0.7	15.4 ± 0.7
$\mu^- \omega$	5.9 ± 0.1	6.2 ± 0.1	19.3 ± 0.6	30.3 ± 0.8
$e^- \omega$	6.1 ± 0.1	6.5 ± 0.1	20.4 ± 0.7	32.5 ± 1.3
$\mu^- K^{*0}$	4.5 ± 0.4	4.5 ± 0.4	13.8 ± 0.3	14.4 ± 0.4
$e^- K^{*0}$	4.3 ± 0.1	5.1 ± 0.1	12.9 ± 0.3	18.0 ± 0.4
$\mu^- \bar{K}^{*0}$	4.7 ± 0.1	4.4 ± 0.1	14.0 ± 0.3	15.0 ± 0.3
$e^- \bar{K}^{*0}$	4.6 ± 0.1	4.9 ± 0.1	12.6 ± 0.6	17.8 ± 0.5
$\mu^- \rho^0$	5.6 ± 0.1	5.0 ± 0.1	13.9 ± 0.4	15.9 ± 0.4
$e^- \rho^0$	4.7 ± 0.1	6.3 ± 0.1	14.5 ± 0.4	17.4 ± 0.5

BACKGROUND ESTIMATION

After all selections, a few events remain in the region $-10\sigma_{M_{\ell V^0}}^{\text{low}} < M_{\ell V^0} < 10\sigma_{M_{\ell V^0}}^{\text{high}}$ and $-10\sigma_{\Delta E}^{\text{low}} < \Delta E < 3\sigma_{\Delta E}^{\text{high}}$, which we define as a background region. This region will be used to estimate the expected background and is shown in Fig. 3. Table III lists the numbers of events in the background region excluding the signal region. The background is efficiently suppressed by the event selection. The comparison between the data and MC shows reasonable agreement for all modes, except for

TABLE III: Number of events in the background region excluding the signal region for data and MC.

Mode	Data	MC
$\tau^- \rightarrow$		
$\mu^- \phi$	2	1.72 ± 1.23
$e^- \phi$	2	$0 \pm_{-0}^{1.19}$
$\mu^- \omega$	7	10.46 ± 1.91
$e^- \omega$	0	1.07 ± 0.62
$\mu^- K^{*0}$	3	3.78 ± 1.72
$e^- K^{*0}$	1	2.26 ± 1.26
$\mu^- \bar{K}^{*0}$	2	1.21 ± 0.92
$e^- \bar{K}^{*0}$	0	0.31 ± 0.31
$\mu^- \rho^0$	12	4.82 ± 1.25
$e^- \rho^0$	0	0.36 ± 0.36

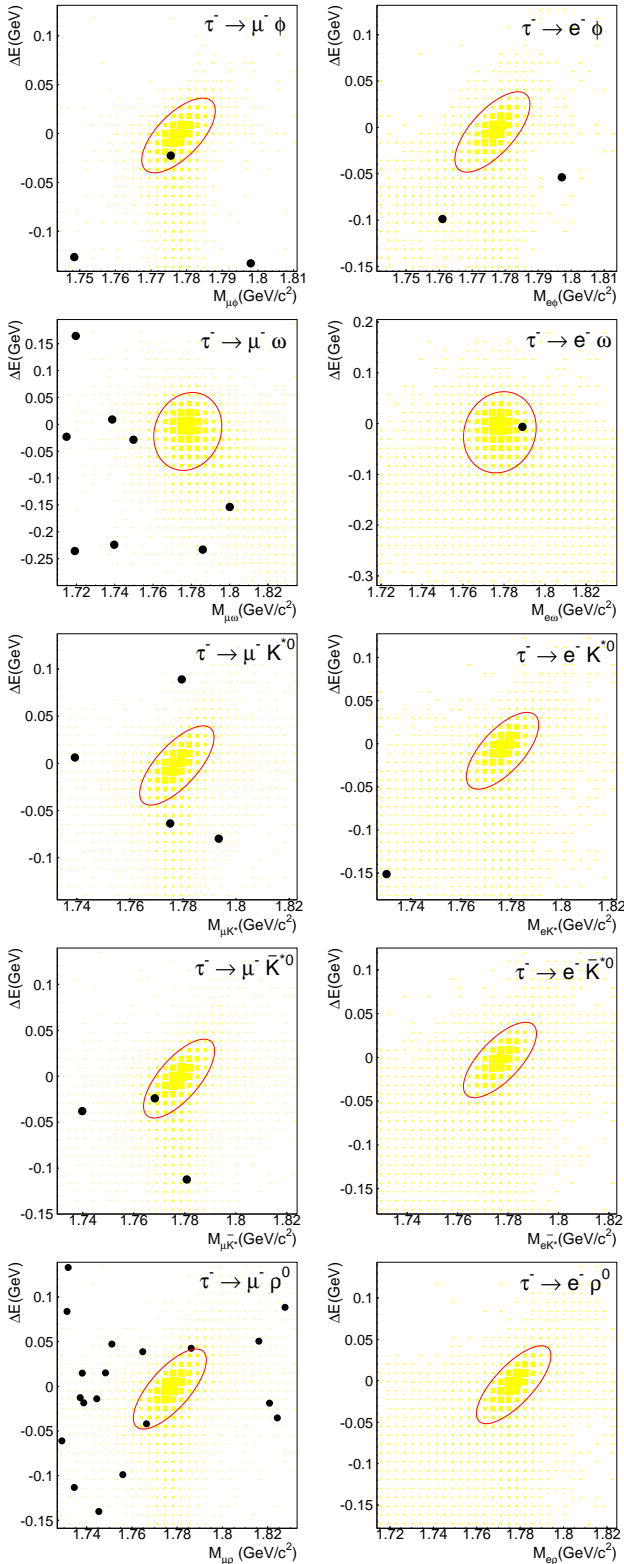


FIG. 3: Distributions of $\Delta E - M_{\ell V^0}$ in the $\pm 10\sigma$ box for (a) $\tau^- \rightarrow \mu^- \phi$, (b) $\tau^- \rightarrow e^- \phi$, (c) $\tau^- \rightarrow \mu^- \omega$, (d) $\tau^- \rightarrow e^- \omega$, (e) $\tau^- \rightarrow \mu^- K^{*0}$, (f) $\tau^- \rightarrow e^- K^{*0}$, (g) $\tau^- \rightarrow \mu^- \bar{K}^{*0}$, (h) $\tau^- \rightarrow e^- \bar{K}^{*0}$, (i) $\tau^- \rightarrow \mu^- \rho^0$ and (j) $\tau^- \rightarrow e^- \rho^0$ after all selections. Dots are data and filled boxes show the signal MC. The elliptical area is the 3σ signal region.

the $\tau^- \rightarrow \mu^- \rho^0$ mode. For this mode one of the dominant background sources is $q\bar{q}$, which at low multiplicity is poorly described by MC. For all other modes we estimate the number of background events in the signal ellipse from the data in the background region using the following method.

Since for most of the modes there are single events only in the $\Delta E - M_{\ell V^0}$ plane both in the data and MC, we first study the background distribution in a sideband region larger than the background region ($1.5 \text{ GeV}/c^2 < M_{\ell V^0} < 1.95 \text{ GeV}/c^2$ and $-0.5 \text{ GeV} < \Delta E < 0.5 \text{ GeV}$) and find that the distribution of events in it is approximately flat in the background region. Therefore we assume that this distribution is flat inside the background region and estimate the expected number of background events in the signal region from the number of data events in the background region times the ratio of the areas of the signal ellipse and background region. If the number of data events in the background region is zero, we assign an upper limit of 2.44 events at the 90% confidence level. The expected number of background events obtained by this method is shown in the third column of Table IV.

For the $\mu^- \omega$ mode, where the number of events is larger, we estimate the background contribution in the signal region using the shape of the background MC distribution normalized to the data yield in the sideband region of the background region.

For the $\mu^- \rho^0$ mode, the background events in Fig.3 come mostly from $\tau^- \rightarrow \pi^- \pi^+ \pi^- \nu$ decay and $q\bar{q}$ when one of the pions is misidentified as a muon. To estimate the background contribution we select a special event sample requiring $P_\mu < 0.1$ for muon candidates instead of $P_\mu > 0.95$. The number of expected background events is then calculated from the product of the number of events with $P_\mu < 0.1$ in the signal region and the muon fake rate.

RESULTS

After unblinding the signal region single events only remain in some modes, see Fig.3. The observed number of events in the signal region is consistent with the expected background. From the numbers of observed events in the signal region and the numbers of expected background events, listed in the second and third columns of Table IV, respectively, we evaluate the upper limit on the number of signal events at the 90% CL, s_{90} , with systematic uncertainties included in the Feldman-Cousins method [16] using the POLE code [17]. In the cases when we give an upper limit of the expected background ($\tau \rightarrow e^- \omega$, $e^- \bar{K}^*$ and $e^- \rho^0$ modes), the number of background events is taken to be zero. This results in conservative upper limits. The main systematic uncertainties on the detection efficiency come from track reconstruction (1.0% per track), electron identification (2.2%),

muon identification (2.0%), kaon/pion separation (1.4% for ϕ reconstruction, 1.1% for K^{*0} and 1.5% for ρ^0), π^0 reconstruction (4.0%), statistics of the signal MC (1.3% for $\ell^-\phi$, 0.7% for $\ell^-\omega$, 0.6% for ℓ^-K^{*0} and $\ell^-\bar{K}^{*0}$, 0.5% for $\mu^-\rho^0$ and 0.6% for $e^-\rho^0$) and uncertainties in the branching fractions for $\phi \rightarrow K^+K^-$ and $\omega \rightarrow \pi^+\pi^-\pi^0$ (1.2% and 0.8%). The uncertainty in the number of τ -pair events mainly comes from the luminosity measurement (1.6%).

The upper limits on the branching fractions, \mathcal{B} , are calculated as $\mathcal{B} < \frac{s_{90}}{2N_{\tau\tau}\epsilon}$, where $N_{\tau\tau} = 4.99 \times 10^8$, is the total number of the τ -pairs produced and ϵ is the signal efficiency including the branching fractions of $\phi \rightarrow K^+K^-$, $\omega \rightarrow \pi^+\pi^-\pi^0$, $K^{*0} \rightarrow K^+\pi^-$ and $\rho^0 \rightarrow \pi^+\pi^-$ [18]. The resulting upper limits on the branching fractions are summarized in Table IV.

TABLE IV: Summary of the number of observed events N_{obs} , the number of expected background events N_{exp} , detection efficiency ϵ , total systematic error $\Delta\epsilon/\epsilon$, 90% CL upper limit of the number of signal events s_{90} and 90% CL upper limit of the branching fractions \mathcal{B} .

Mode	N_{obs}	N_{exp}	ϵ	$\Delta\epsilon/\epsilon$	s_{90}	UL on \mathcal{B}
$\tau^- \rightarrow$			(%)	(%)		(90% CL)
$\mu^-\phi$	1	0.17 ± 0.12	3.14	5.2	4.17	1.3×10^{-7}
$e^-\phi$	0	0.18 ± 0.12	3.10	5.3	2.27	7.3×10^{-8}
$\mu^-\omega$	0	0.19 ± 0.20	2.51	6.3	2.22	8.9×10^{-8}
$e^-\omega$	1	< 0.24	2.46	6.3	4.34	1.8×10^{-7}
μ^-K^{*0}	0	0.26 ± 0.15	3.71	4.8	2.20	5.9×10^{-8}
e^-K^{*0}	0	0.08 ± 0.08	3.04	4.9	2.35	7.8×10^{-8}
$\mu^-\bar{K}^{*0}$	1	0.17 ± 0.12	4.02	4.8	4.14	1.0×10^{-7}
$e^-\bar{K}^{*0}$	0	< 0.17	3.21	4.9	2.45	7.7×10^{-8}
$\mu^-\rho^0$	1	1.04 ± 0.28	4.89	4.9	3.34	6.8×10^{-8}
$e^-\rho^0$	0	< 0.17	3.94	5.1	2.46	6.3×10^{-8}

SUMMARY

We have searched for the LFV decays $\tau^- \rightarrow \ell^-\phi$, $\ell^-\omega$, ℓ^-K^{*0} , $\ell^-\bar{K}^{*0}$ and $\ell^-\rho^0$ using 543 fb^{-1} of data obtained in the Belle experiment. No evidence for a signal is observed, and the upper limits on the branching fractions are set in the range $(5.9 - 18) \times 10^{-8}$ at the 90% CL. This analysis is the first search for the $\tau^- \rightarrow \ell^-\omega$ mode. The results for the $\tau^- \rightarrow \ell^-\phi$, ℓ^-K^{*0} , $\ell^-\bar{K}^{*0}$ and $\ell^-\rho^0$ modes are 3 – 10 times more restrictive than our previous results obtained using 158 fb^{-1} of data. The sensitivity improvement comes from a factor of 3.4-times larger statistics and an optimized analysis. In particular, we have improved the conditions on p_{miss} and m_{miss}^2 to reduce $\tau\tau$ and $q\bar{q}$ background as well as those on the opening angle α to reduce two-photon background. As a result, better background suppression is achieved and the

efficiency is improved, e.g. it increases by a factor of 2.8 for the $\mu^-\phi$ and 2.5 for the $e^-\phi$ mode. The new upper limits can be used to constrain the parameter space of various scenarios beyond the SM.

ACKNOWLEDGEMENTS

We thank the KEKB group for the excellent operation of the accelerator, the KEK cryogenics group for the efficient operation of the solenoid, and the KEK computer group and the National Institute of Informatics for valuable computing and Super-SINET network support. We acknowledge support from the Ministry of Education, Culture, Sports, Science, and Technology of Japan and the Japan Society for the Promotion of Science; the Australian Research Council and the Australian Department of Education, Science and Training; the National Natural Science Foundation of China under contract No. 10575109 and 10775142; the Department of Science and Technology of India; the BK21 program of the Ministry of Education of Korea, the CHEP SRC program and Basic Research program (grant No. R01-2005-000-10089-0) of the Korea Science and Engineering Foundation, and the Pure Basic Research Group program of the Korea Research Foundation; the Polish State Committee for Scientific Research; the Ministry of Education and Science of the Russian Federation and the Russian Federal Agency for Atomic Energy; the Slovenian Research Agency; the Swiss National Science Foundation; the National Science Council and the Ministry of Education of Taiwan; and the U.S. Department of Energy.

- [1] A. Ilakovac, Phys. Rev. D **62**, 036010 (2000).
- [2] A. Brignole and A. Rossi, Nucl. Phys. B **701**, 3 (2004).
- [3] C.-H. Chen and C.-Q. Geng, Phys. Rev. D **74**, 035010 (2006).
- [4] D.W. Bliss *et al.* (CLEO Collaboration), Phys. Rev. D **57**, 5903 (1998).
- [5] Throughout this paper, the inclusion of the charge-conjugate decay modes is implied unless otherwise stated.
- [6] B. Aubert *et al.* (BaBar Collaboration), arXiv:0711.0980 [hep-ex].
- [7] A. Abashian *et al.* (Belle Collaboration), Nucl. Instr. and Meth. A **479**, 117 (2002).
- [8] S. Kurokawa and E. Kikutani, Nucl. Instr. and Meth. A **499**, 1 (2003), and other papers included in this volume.
- [9] Y. Yusa *et al.* (Belle Collaboration), Phys. Lett. B **640**, 138 (2006).
- [10] Z. Natkaniec *et al.* (Belle SVD2 Group), Nucl. Instr. and Meth. A **560**, 1 (2006).
- [11] S. Jadach, B.F.L. Ward, Z. Wąs, Comp. Phys. Commun. **130**, 260 (2000).
- [12] D. J. Lange, Nucl. Instr. and Meth. A **462**, 152 (2001).
- [13] F.A. Berends, P.H. Daverveldt, R. Kleiss, Comp. Phys. Commun. **40**, 285 (1986).

- [14] CERN Program Library Long Writeup No. W5013, 1993.
- [15] K. Hanagaki *et al.*, Nucl. Instr. and Meth. A **485**, 490 (2002); A. Abashian *et al.*, Nucl. Instr. and Meth. A **491**, 69 (2002); E. Nakano, Nucl. Instr. and Meth. A**494**, 117 (2002).
- [16] G. J. Feldman and R. D. Cousins, Phys. Rev. D **57**, 3873 (1998).
- [17] The Highland-Cousins method for calculating upper limits with systematic errors is described in J. Conrad *et al.*, Phys. Rev. D **67**, 012002 (2003).
- [18] W.-M. Yao *et al.* (Particle Data Group), J. Phys. G **33**, 1 (2006).